Supporting Information

High-Temperature Dielectric Energy Storage Materials Fabricated by Crosslinking Titanium Dioxide and Polyarylene Ether Nitrile

Yujie Feng, Shumin Bao, Zaixing Wang, Yongxian Liu, Yayao Jiao, Lingling Wang *, Xiufu Hua * and Renbo Wei *

School of Chemical Engineering, Northwest University, Xi'an 710069, China.

E-mail addresses: wangll@nwu.edu.cn (L.W.); huaxf@nwu.edu.cn (X.H.); weirb10@nwu.edu.cn (R.W.)

Finite element Calculation Simulation: The phase field simulation for evolution of conductive channel was conducted as previously reported. A dimensionless phase field variable *s* (*x*, *t*) was introduced to characterize the breakdown state of the materials, where the value of s varies from 0 to 1, representing the undamaged state *(s*=1*)* and the completely breakdown state *(s*=0*)*, respectively.When it was in any of the middle states, the dielectric constant εr can be calculated as follows:

$$\varepsilon(s) = \frac{\varepsilon_0}{f(s)+\eta} \quad \text{(Eq. S1)}$$

where $f(s) = 4s^3 - 3s^4$. ε_0 is the initial ε_r, and η is set as 0.001.

Integrating the entire space Ω occupied by the dielectric gives the energy function of the system:

$$\Pi[s,\Phi] = \int_\Omega \left[-\frac{\varepsilon(s)}{2}\nabla\Phi\cdot\nabla\Phi + \Gamma\frac{1-f(s)}{l^2} + \frac{\Gamma}{4}\nabla s\cdot\nabla s \right] dV \quad \text{(Eq. S2)}$$

where Γ and Φ is breakdown energy, and electric potential, respectively. When the electrostatic energy required to extend the conductive branch per unit length is more than the minimum energy Γ required for breakdown, a conductive channel emerges and propagates.The breakdown failure process is represented by a law of linear dynamic supposing the ratio of damage rate to energy driving force:

$$\frac{\partial s}{\partial t} = -\frac{m\delta\Pi}{\delta s} \quad \text{(Eq. S3)}$$

Thus, the evolution equation for the damage variable s can be obtained after substituting in the detailed forms of the energy functions:

$$\frac{1}{m}\frac{\partial s}{\partial t} = \frac{\varepsilon^{'}(s)}{2}\nabla\Phi\cdot\nabla\Phi + \frac{\Gamma}{l^2}f^{'}(s) + \frac{\Gamma}{2}\nabla^2 s \quad \text{(Eq. S4)}$$

where, the mobility m is used to characterize the damage diffusivity in composite. To facilitate numerical calculation,we will normalize all lengths by *l*, energies by *Γl*, time by *mΓl*, and electric pontentials by $\sqrt{\Gamma/\varepsilon^0}$. the resulting dimensionless governing equations:

$$\bar{\nabla}\cdot\left[\frac{1}{f(s)+\eta}\ \bar{\nabla}\ \bar{\Phi}\right] = 0 \quad \text{(Eq. S5)}$$

$$\frac{\partial s}{\partial t} = -\frac{f^{'}(s)}{2|f(s)+\eta|}\ \bar{\nabla}\ \bar{\Phi}\ \cdot\bar{\nabla}\ \bar{\Phi} + f^{'}(s) + \frac{1}{2}\ \bar{\nabla}^2 s \quad \text{(Eq. S6)}$$

In which the symbols with over-bars are the dimensionless counterparts of the corresponding quantities.

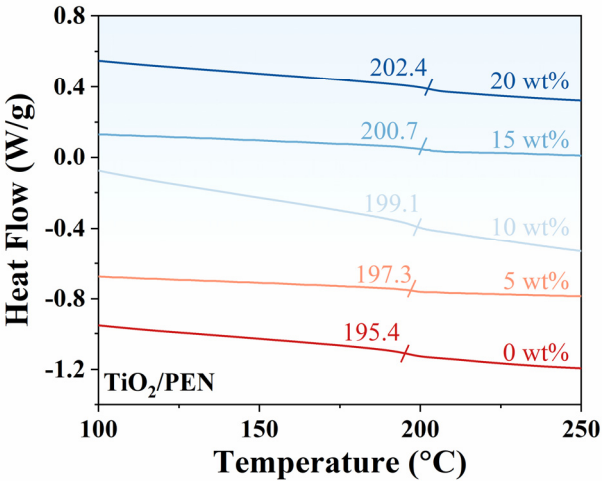

Figure S1. DSC curves of TiO_2/PEN nanocomposites.

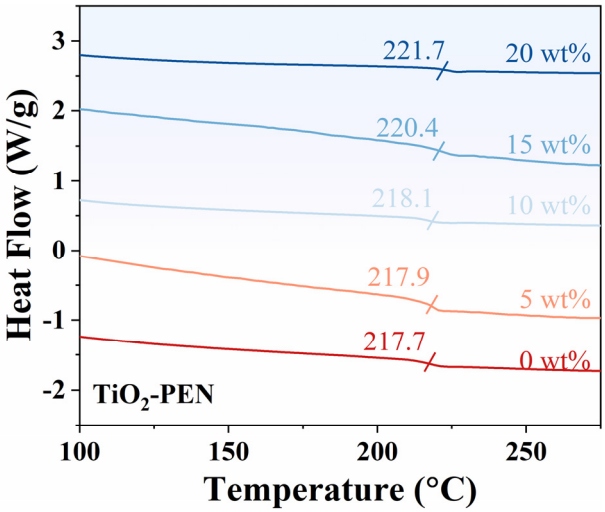

Figure S2. DSC curves of TiO_2-PEN hybrids.

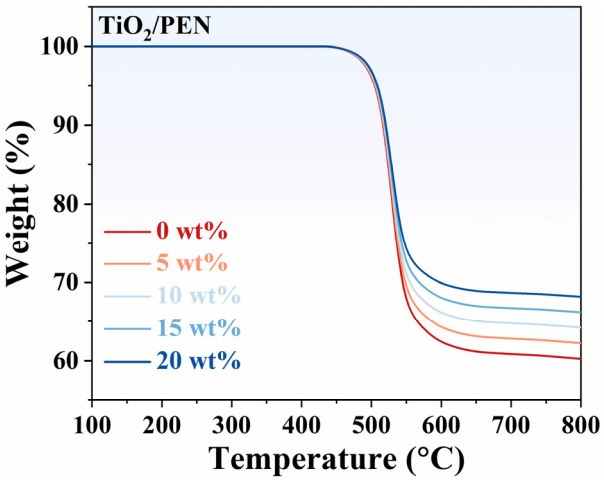

Figure S3. TGA curves of TiO_2/PEN nanocomposites.

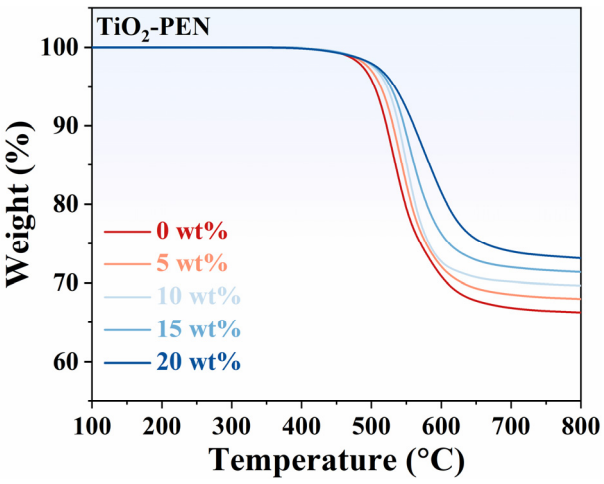

Figure S4. TGA curves of TiO_2-PEN hybrids.

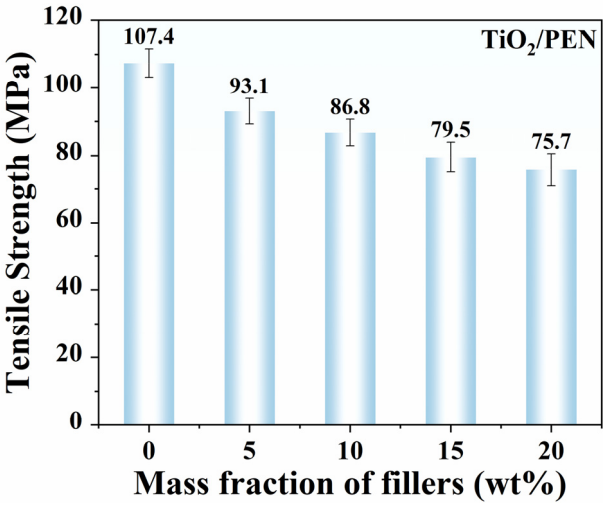

Figure S5. Tensile strength of TiO_2/PEN nanocomposites.

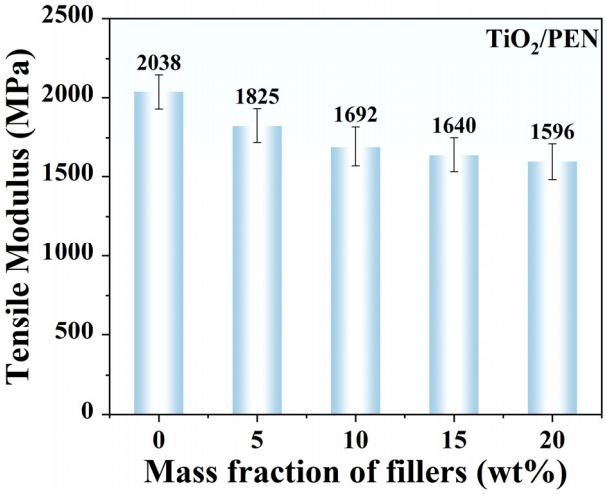

Figure S6. Tensile modulus of TiO_2/PEN nanocomposites.

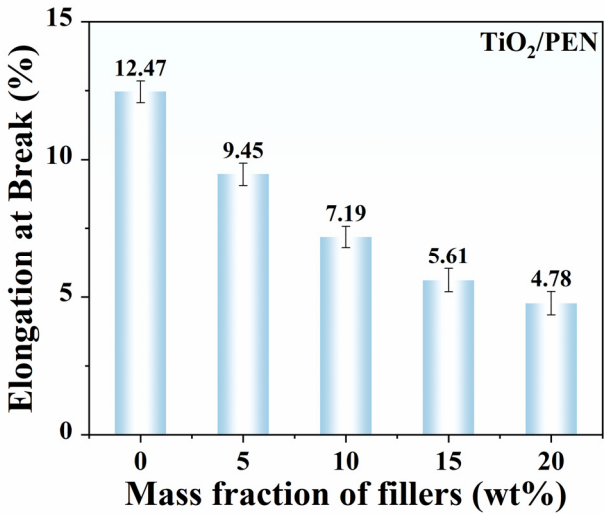

Figure S7. Elongation at break of TiO_2/PEN nanocomposites.

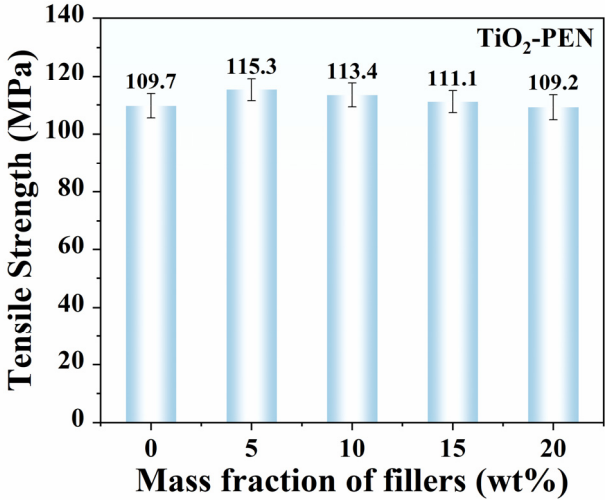

Figure S8. Tensile strength of TiO_2-PEN hybrids.

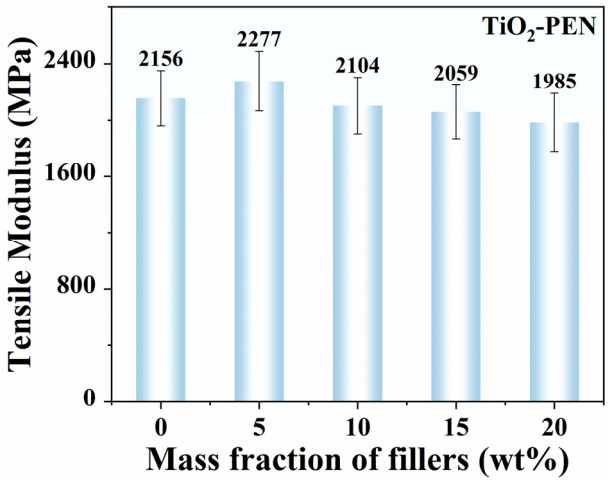

Figure S9. Tensile modulus of TiO_2-PEN hybrids.

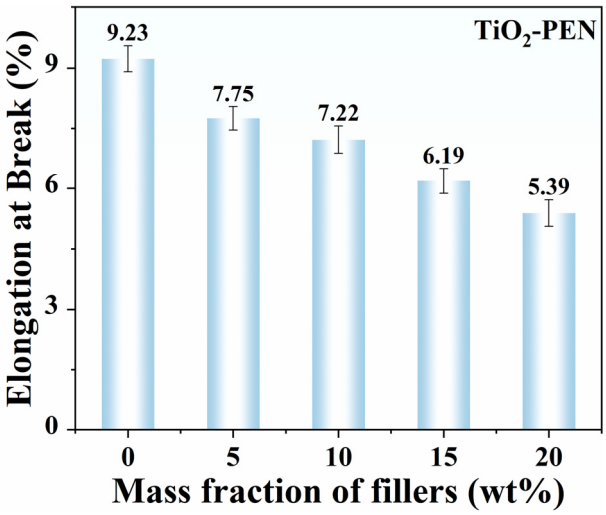

Figure S10. Elongation at break of TiO_2-PEN hybrids.

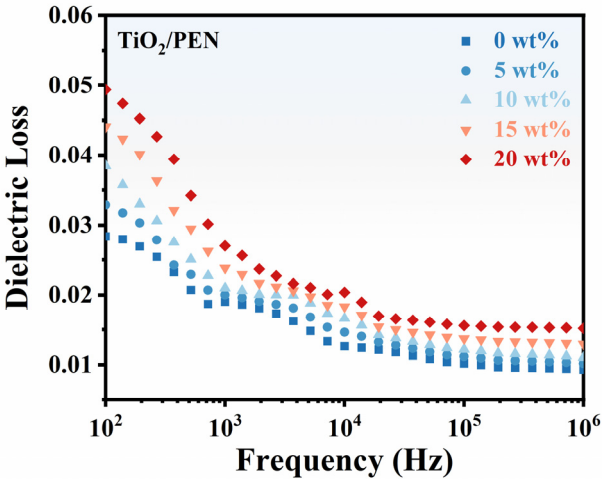

Figure S11. Dielectric loss of TiO_2/PEN nanocomposites.

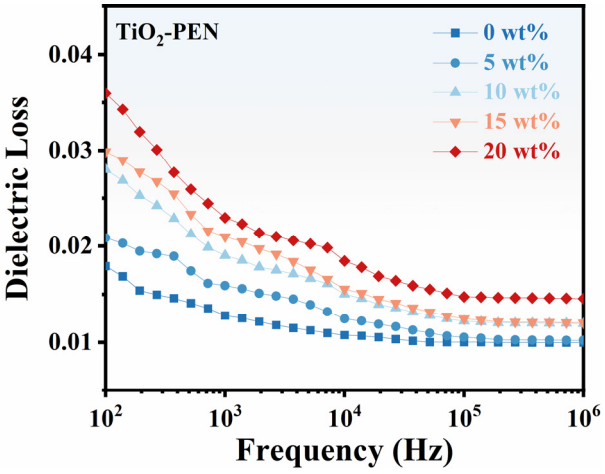

Figure S12. Dielectric loss of TiO_2-PEN hybrids.

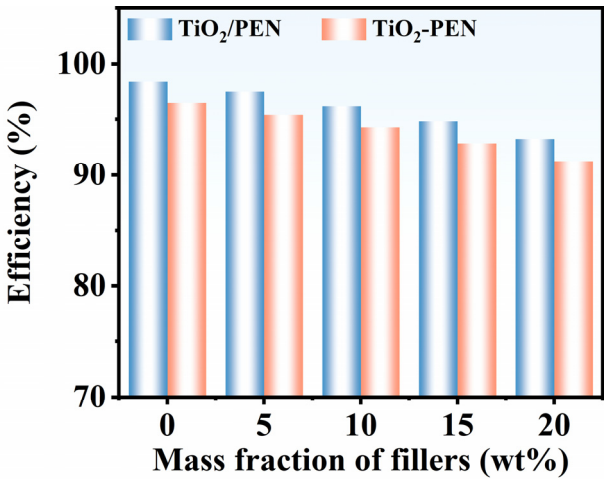

Figure S13. Efficiency of TiO_2/PEN nanocomposites and TiO_2-PEN hybrids.

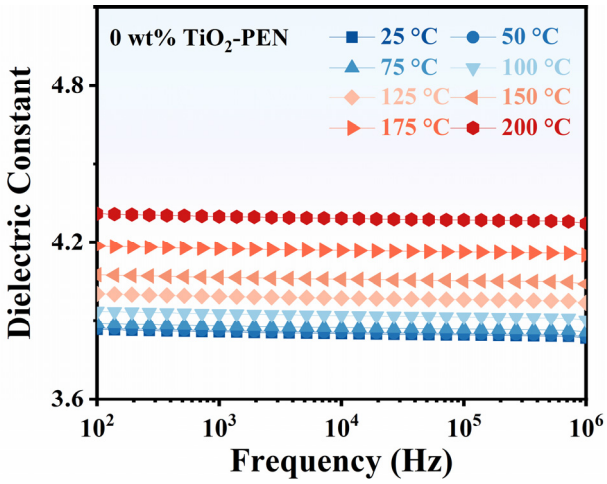

Figure S14. Dielectric constant of 0 wt% TiO_2-PEN at different temperatures.

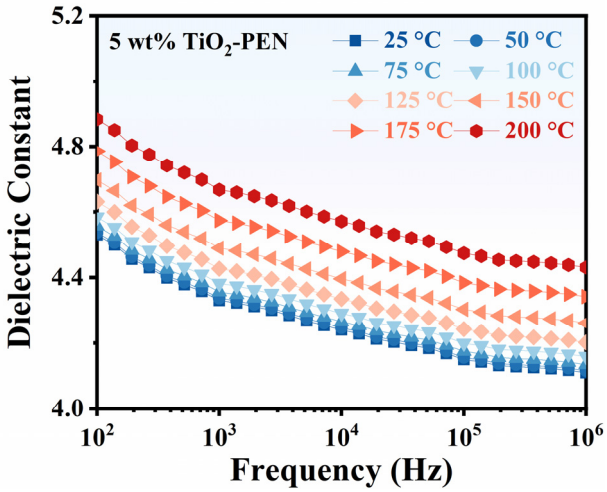

Figure S15. Dielectric constant of 5 wt% TiO_2-PEN at different temperatures.

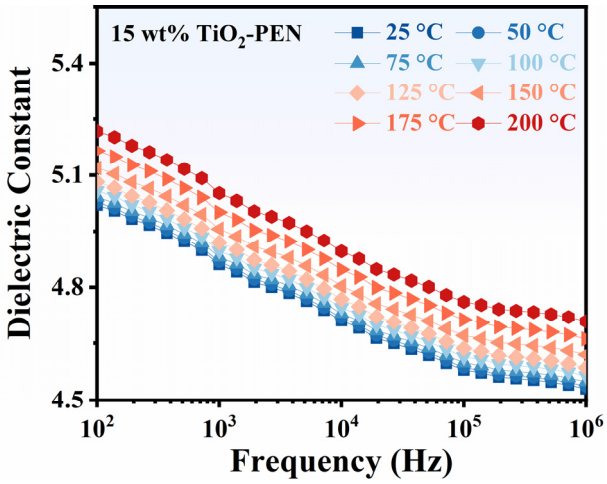

Figure S16. Dielectric constant of 15 wt% TiO_2-PEN at different temperatures.

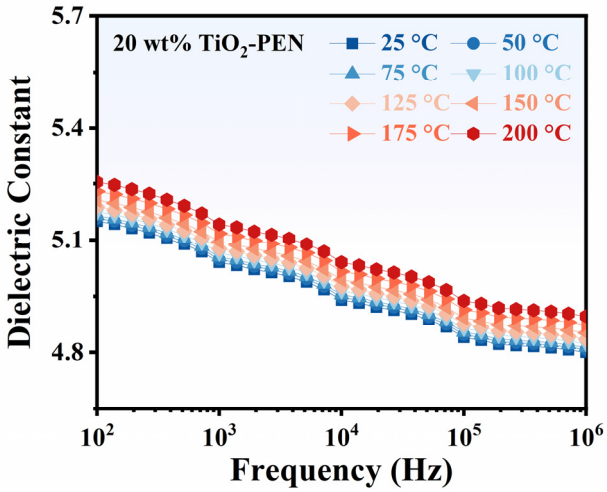

Figure S17. Dielectric constant of 20 wt% TiO_2-PEN at different temperatures.

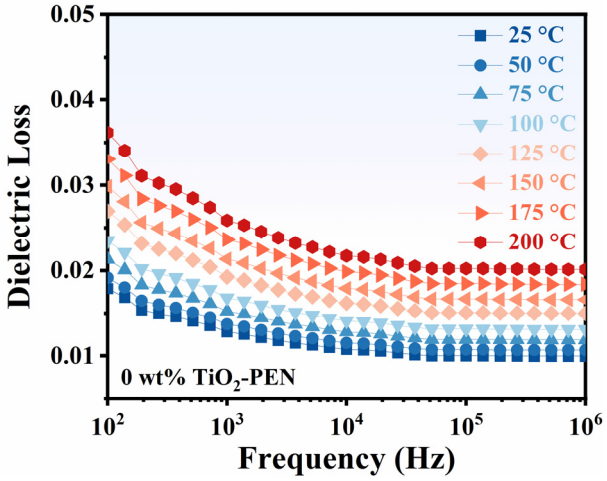

Figure S18. Dielectric loss of 0 wt% TiO_2-PEN at different temperatures.

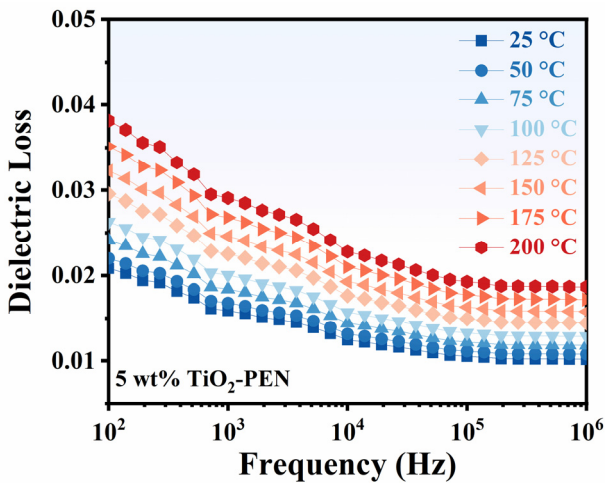

Figure S19. Dielectric loss of 5 wt% TiO_2-PEN at different temperatures.

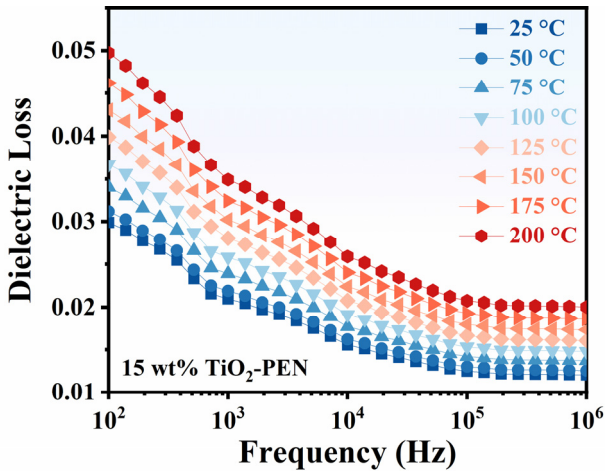

Figure S20. Dielectric loss of 15 wt% TiO_2-PEN at different temperatures.

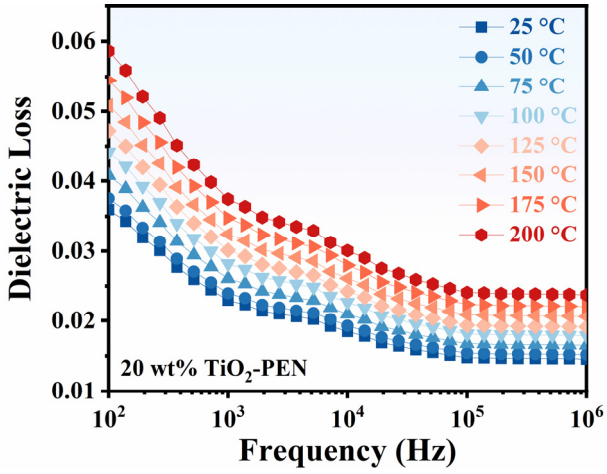

Figure S21. Dielectric loss of 20 wt% TiO_2-PEN at different temperatures.

Table S1. Properties of TiO_2/PEN nanocomposites.

	0 wt%	5 wt%	10 wt%	15 wt%	20 wt%
Glass transition temperature (T_g, °C)	195.4	197.3	199.1	200.7	202.4
Decomposition temperature ($T_{10\%}$,°C)	516.7	517.7	518.7	519.7	520.6
Residue weight at 800 °C (W_{800}, %)	60.1	62.3	64.2	66.1	68.2
Tensile strength (MPa)	107.4	93.1	86.8	79.5	75.7
Tensile modulus (MPa)	2038	1825	1692	1640	1596
Elongation at break (%)	12.47	9.45	7.19	5.61	4.78
Dielectric constant at 1000 Hz (ε_r)	3.96	4.34	4.5	4.61	4.72
Breakdown strength (E_b, kV/mm)	227.5	212.7	207.2	202.1	197.3
Discharged energy density (U_d, J/cc)	0.56	0.60	0.62	0.62	0.63
Discharged energy efficiency (η, %)	98.4	97.5	96.2	94.8	93.3

Table S2. Properties of TiO_2-PEN hybrids.

	0 wt%	5 wt%	10 wt%	15 wt%	20 wt%
Glass transition temperature (T_g, °C)	217.7	217.9	218.1	220.4	221.7
Decomposition temperature ($T_{10\%}$,°C)	521.7	531.2	539.1	547.1	560.9
Residue weight at 800 °C (W_{800}, %)	66.3	67.9	69.6	71.4	73.1
Tensile strength (MPa)	109.7	115.3	113.4	111.1	109.2
Tensile modulus (MPa)	2156	2277	2104	2059	1985
Elongation at break (%)	9.23	7.75	7.22	6.19	5.39
Dielectric constant at 1000 Hz (ε_r, 25 °C)	3.86	4.33	4.67	4.86	5.04
Breakdown strength (E_b, 25 °C, kV/mm)	224.8	212.4	204.8	199.4	194.3
Discharged energy density (U_d, 25 °C, J/cc)	0.53	0.59	0.63	0.65	0.65
Discharged energy efficiency (η, 25 °C, %)	96.5	95.4	94.3	92.9	91.3
Dielectric constant at 1000 Hz (ε_r, 150 °C)	4.07	4.49	4.79	4.96	5.09
Breakdown strength (E_b, 150 °C, kV/mm)	208.1	198.4	192.7	187.2	181.9
Discharged energy density (U_d, 150 °C, J/cc)	0.54	0.59	0.60	0.61	0.62
Discharged energy efficiency (η, 150 °C, %)	93.6	92.4	91.0	89.2	87.1

Table S3. Comparison of the composites characteristics with those in the literature.

Sample	ε_r	Tanδ	E_b (kV/mm)	η (%)	U_e (J/cm^3)	T_g (℃)	reference
TiO_2-PEN	5.04	0.021	194.3	91.3	0.84	221.7	This work
TiO_2/PEN	4.72	0.027	197.3	93.3	0.81	202.4	This work
CCTO/PEN	4.99	0.038	168.8	/	0.63	/	[1]
PENS100	3.60	0.018	203.5	/	0.68	180.0	[2]
TR-PEN200	4.11	0.020	220.7	/	0.89	222.9	[3]
CCTO15-PEN	6.27	0.027	162.4	/	0.78	/	[4]
PENK2	4.07	0.013	191.2	/	0.66	216.2	[5]
BT@CuPc/PEN	5.41	0.017	187.2	/	0.82	217.1	[6]
BT@PANI/PEN	4.55	0.013	208.5	/	0.78	216.4	[7]

References

[1] F Gao, R Wei, L Zhou, W Luo, Z Li, L Pang, S Li, X Hua. L Wang, Improved dielectric properties of poly(arylene ether nitrile) with sulfonated poly(arylene ether nitrile) modified $CaCu_3Ti_4O_{12}$, Polym Compos, 2023, 44, 8658-8668.

[2] W Hu, Y You, L Tong, L Tu, Y Wang, R Wei, X Liu. Preparation and physical properties of polyarylene ether nitrile and polyarylene ether sulfone random copolymers, High Perform Polym, 2018, 31, 686-693.

[3] Y You, S Liu, L Tu, Y Wang, C Zhan, X Du, R Wei, X Liu. Controllable fabrication of poly(arylene ether nitrile) dielectrics for thermal-resistant film capacitors, Macromolecules, 2019, 52, 5850-5859.

[4] L Zhou, Z Zhang, Y Feng, F Gao, Y Luo, S Li, R Wei, L Wang. Covalently cross-linked $CaCu_3Ti_4O_{12}$ and poly(arylene ether nitrile) hybrids with enhanced high temperature energy storage properties, Mater Today Commun, 2024, 38, 108544.

[5] H Mao, Y You, L Tong, X Tang, R Wei, X Liu. Dielectric properties of deblock copolymers containing a polyarylene ether nitrile block and a polyarylene ether ketone block, J Mater Sci-Mater Electron, 2017, 29, 3127-3134.

[6] Y You, W Han, L Tu, Y Wang, R Wei, X Liu. Double-layer core/shell-structured nanoparticles in polyarylene ether nitrile-based nanocomposites as flexible dielectric materials, RSC Adv 2017, 7, 29306-29311.

[7] R Wei, Q Huo, K Liu, AY Elnaggar, SM El-Bahy, ZM El-Bahy, J Ren, L Wang, Z Wu. Distributing fluorinated carbon nanotube on pore walls of polyarylene ether nitrile porous films for advanced electromagnetic interference shielding, Adv Compos Hybrid Mater, 2024, 7, 196.